ASTRONOMY & ASTROPHYSICS
SUPPLEMENT SERIES

DECEMBER II **1996**, PAGE 587

Astron. Astrophys. Suppl. Ser. **120,** 587-602 (1996)

Determination of interstellar helium parameters from the ULYSSES-NEUTRALGAS experiment: Method of data analysis

M. Banaszkiewicz*, M. Witte and H. Rosenbauer

Max-Planck-Institut für Aeronomie, D-37189 Katlenburg-Lindau, Germany

Received October 11, 1995; accepted April 24, 1996

Abstract. — The GAS instrument on board the ULYSSES spacecraft has, for the first time, measured directly the interstellar flux of helium atoms in the inner solar system. From the locally measured angular distribution of the flux, the task is to derive the five parameters of the Maxwellian distribution function: density, bulk velocity vector, and temperature describing the state of the interstellar helium outside of the heliosphere, "at infinity". To accomplish this, a new method for the data analysis has been developed that employs Tarantola's approach. In the inverse problem considered a solution is found by optimizing (minimizing) the sum of squared residuals between the measured counts and the count numbers derived from a computer simulation. The mathematical formulation of this method is described in detail. The method proved to be reliable and robust in that it always finds a solution. In two extreme, but still typical cases of actual measurements the power but also the limitations of the method are demonstrated. The solution obtained can either be unique, e.g. for measurements taken in the helium cone at 1.5 AU, or belongs, in cases of larger heliocentric distances and outside of the cone, to a one-dimensional family of equally acceptable helium parameters. To obtain a unique solution in the latter, ill-determined problem, further information is required, which can be achieved by combining measurements that are taken during sufficiently different conditions, e.g. downwind or crosswind with respect to the helium flow (comparable to the tomography problem). Three different approaches to this problem have been investigated. The confidence factor of a solution is estimated by a standard χ^2 test and the error bars are determined from the covariance matrix. Also, the dependence of the solutions on systematic errors in a number of input parameters, such as background level, ionization rate, spacecraft attitude and efficiency function of the detector is studied.

Key words: ISM: atoms — interplanetary medium — methods: observational, data analysis

1. Introduction

Interstellar neutral atoms which penetrate the Solar System carry important information about the density, velocity, and temperature of the local interstellar medium (LISM). Fluxes of neutral hydrogen and helium have been indirectly observed for more than twenty years by means of resonantly scattered solar UV light (see e.g. Lallement 1990; Chassefière et al. 1990). Further evidence of interstellar neutrals is provided by pick-up He and H ions that originate from the interstellar neutral atoms after ionization by photons or solar wind particles (Möbius 1990). Both methods do not measure directly the neutral fluxes but rather the secondary effects connected with inflowing atoms. The LISM parameters are then extracted from variations of resonant line glow or pick-up ion density with the observer's position in the Solar System. Yet another method of determining the interstellar medium parameters employs observations of Doppler-shifted absorption lines in the nearby stars (Frisch 1990; Lallement 1993). In this approach, however, the LISM characteristics are averaged over large distances.

The first attempt to measure the neutral gas fluxes directly and in-situ has been made by the MPAe group which launched the Neutral-Gas Experiment on board the Ulysses spacecraft (Rosenbauer & Fahr 1977; Witte et al. 1991, 1993). In their method the inflowing neutral atoms hit the surface covered by lithium fluoride (LiF) and sputter ions and electrons which are registered in two different operational modes by channeltrons. As this instrument acts as a pin-hole camera the instrumental effects are reduced to the efficiency function of the detector which corresponds to the probability that an incoming neutral atom

Send offprint requests to: M. Witte

*Permanent address: Space Research Centre, Bartycka 18[a], 00–716 Warszawa, Poland

is registered. The measured count rates depend on the direction of observation - they are largest when the detector points towards the local bulk flow of neutrals and decrease to the background value over an angular distance corresponding to a few thermal widths of the helium distribution function. From the direction, intensity and spread of the flux one can determine velocity, density, and temperature of the interstellar neutral gas. However, from the constituents of the neutral gas, only the helium component can be efficiently observed because of the relative energy and the local densities of the other components (see Sect. 4.6).

The so-called "inverse method" which is explained in general terms in Sect. 3, is based, in our case, on the following considerations. By describing the state of the interstellar helium by a Maxwellian distribution which depends on five parameters (the three components of the bulk velocity vector $\mathbf{v}_{\mathrm{b},\infty}$, the density n_∞, and the temperature T_∞) the evolution of this distribution to the position R of the observer can be calculated simply using Liouville's theorem. This is straightforward as the time dependent radiation pressure can be neglected for helium particles (this would not be true for hydrogen particles). Losses due to photoionization are taken into account by a constant parameter. The local distribution is then convolved with the instrumental functions (geometric factor, efficiency function depending on the relative velocity of the helium parameters in the instrument reference system, and the angular grid of observation) resulting in a simulated angular distribution which can be directly compared with the observed one. In a five-dimensional fitting process the five parameters are varied independently until the difference (the residual) between the simulated and observed distribution reaches an absolute minimum (see Sect. 3). The set of five parameters corresponding to this minimum is regarded as a solution, i.e. it defines the Maxwellian distribution at infinity which matches the observations in the best possible way.

The pre-mission simulations (Banaszkiewicz et al. 1990) as well as processing of the first data sets (Witte et al. 1993) showed that for the assumed Maxwellian velocity distribution of neutrals far away from the Sun it is possible to derive its most important moments by applying this inverse method. Since then the experimental data base has increased significantly and new interesting cases have been found. The computer code has been extensively tested and refined to deal with the situations when the determination of parameters might be ambiguous. In this paper we present the details of the method and show how it works on two exemplary data sets. The results of the analysis of all in-ecliptic data sets as well as implications for the physics of the LISM will be given in forthcoming papers (Witte et al. 1996).

The outline of the paper is as follows. We begin with a concise description of the experimental set-up and introduce a formula for the measured count numbers. Then we describe the inverse method, which was adapted from Tarantola (1987), and specify it for our problem. Next, we present the important numerical points of the algorithm and discuss its accuracy. Later, we apply the method to two qualitatively different data sets and explain how we deal with ill-conditioned problems. We also show how the results depend on input parameters (ionization rate, background value, etc.) which are free parameters of the problem and have to be determined from other sources. Finally we discuss our assumptions, confidence limits of the method and how its results relate to those obtained from other methods.

2. Definition of the experimental parameters

The experimental set-up and the technical details of the instrument have been presented in detail by Witte et al. (1990). In this paper we use only data obtained in the operational mode, in which the secondary ions are registered which are emitted from the LiF-surface after impacts of neutral particles. The other mode, in which secondary electrons are counted, is useful for measurements of the UV-intensity distribution, which are not the subject of this paper.

In the following we describe briefly those instrumental issues which are relevant to the data evaluation of the neutral particles. Since the GAS device works, in principle, as a pin-hole camera, the flux of neutrals in a given direction is represented by a count number. The probability to register a neutral particle which reaches the detector is given by an energy dependent efficiency function $f_{\mathrm{eff}}(E)$ (Fig. 1). During one rotation period of Ulysses (12 s) the detector scans a ring on the celestial sphere at a given elevation angle measured with respect to the spin axis which points towards Earth (Fig. 2). Usually this angle ϵ is changed every $T_{\mathrm{s}} = 68$ min by means of a mechanical stepping platform with a constant step width of $\Delta\epsilon$, selectable by telecommand to be $1°, 2°, 4°$, or $8°$. The observational range of the rotation angle (azimuth) can be chosen as $360°$, $90°$, $45°$, or $22.^{\circ}5$ and is always divided into 32 azimuthal sectors with a width of $\Delta\alpha = 11.^{\circ}2$, $2.^{\circ}8$, $1.^{\circ}4$, or $0.^{\circ}7$, respectively. This scheme allows the whole celestial sphere or subsections in many different angular ranges and angular resolutions to be subsequently scanned to optimize the observational conditions. In this way the whole scanned area of the sky is divided, in a natural way, into segments (pixels) with angular dimensions $\Delta\epsilon \times \Delta\alpha$. Their centers are given by varying step-by-step elevation angles ϵ_i and the center points of 32 azimuthal sectors α_j. As the spacecraft rotates, the counts in the pixel (ϵ_i, α_j) are collected from the azimuthal range $[\alpha_j - 0.5\Delta\alpha, \alpha_j + 0.5\Delta\alpha]$ which corresponds to the motion of the optical axis of the instrument. Due to this motion, the picture composed of pixels is "smeared" and neighboring pixels have an overlap of half a field of view, each. For any direction of the

optical axis, only particles are accepted which enter the instrument with an angle θ inside the field of view (Fig. 3). The GAS device employs two independent channels with parallel optical axes different only in their fields of view: $\pm 3\overset{\circ}{.}7$ half-cone angle $\theta_{\max}$ for the wide field of view (WFOV) and $\pm 2\overset{\circ}{.}45$ for the narrow field of view (NFOV). The effective area S of the detector for particles entering along the optical axis ($\theta = 0°$) is $S_0 = 0.0908\,\mathrm{cm}^2$, for other directions $S = G(\theta)\ S_0$, with the geometric instrumental function $0 \leq G(\theta) \leq 1$ (Fig. 3).

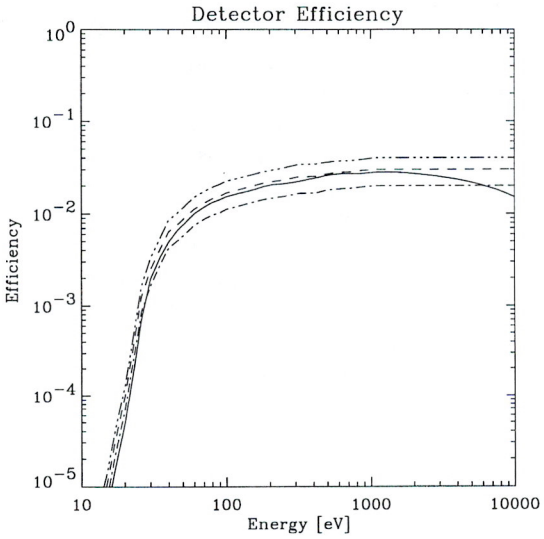

Fig. 1. Efficiency functions of the detector for helium atoms: the standard model is obtained by a fit to all calibration points (solid line). A second model is obtained from an upper envelope of calibration data (dashed line), and its upper (dashed-triple_dotted line) and lower (dashed-dotted line) limits assumed to be larger (smaller) by 30%, are shown

The elevation and azimuth angles define the direction in the spacecraft system of coordinates. The transformation matrix T from the ecliptic to s/c coordinate system is calculated from the position of Ulysses, its spin axis orientation, and the position of the Sun, which is at azimuth 270°, by definition. The required data are provided in navigational data files with a time increment of 3 hours. The changes of the spacecraft position and velocity during one standard elevation scan T_s are small, typically $\approx$ 1 10^{-4} AU and 0.005 km/s, respectively, and therefore are neglected.

With these definitions, the relationship between the distribution function and the count rate in a pixel is given in the following way: the number density of particles coming with the velocity $\mathbf{v}$ to the point $\mathbf{r}$ is $F(\mathbf{v};\mathbf{r})\ \mathrm{d}^3v$, where F is the velocity distribution function of neutrals in the ecliptic coordinate system. The differential flux of atoms approaching the detector with the relative speed v_{rel} is $v_{\mathrm{rel}}\ F(\mathbf{v};\mathbf{r})\ \mathrm{d}^3v$. Only a fraction $f_{\mathrm{eff}}(E_{\mathrm{rel}})\ G(\theta)$ of particles with energy $E_{\mathrm{rel}} = \frac{mv_{\mathrm{rel}}^2}{2}$ will be registered and thus

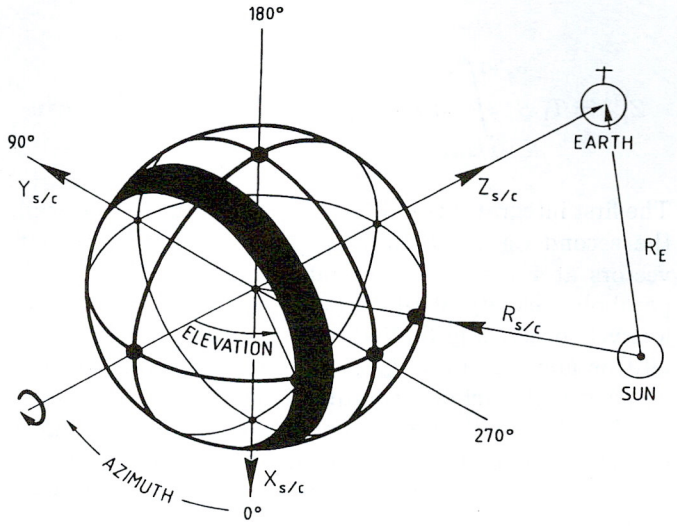

Fig. 2. The relationship between the spacecraft coordinate systems $x_{\mathrm{s/c}}, y_{\mathrm{s/c}}, z_{\mathrm{s/c}}$ (elevation (ϵ) and azimuth (α) angles) and the solar ecliptic coordinate system, when the position of Earth R_{E} and of the spacecraft $R_{\mathrm{s/c}}$ are given in ecliptic coordinates. By definition, the Sun is in the $-y/z$ - quadrant

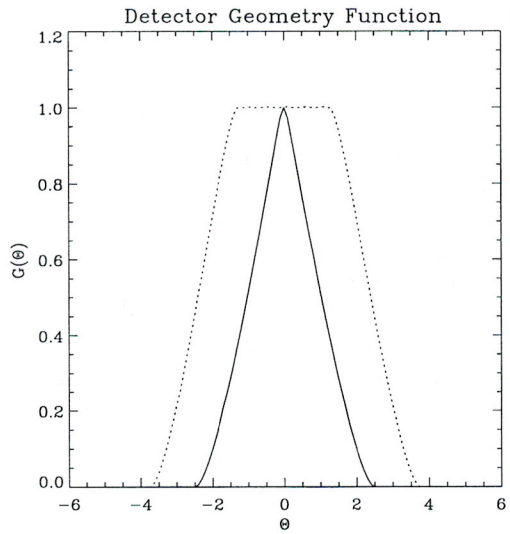

Fig. 3. The detector geometry function $G(\theta)$ for the narrow (solid) and wide (dotted) fields of view; the angle θ is measured from the optical axis of the instrument

contribute to the number of counts $Z(\mathbf{v})$ observed during a given integration time T_{I}:

$$Z(\mathbf{v})\ \mathrm{d}^3v = T_{\mathrm{I}}\ S\ f_{\mathrm{eff}}(E_{\mathrm{rel}})\ G(\theta)\ v_{\mathrm{rel}}\ F(\mathbf{v};\mathbf{r})\ \mathrm{d}^3v \qquad (1)$$

Finally, after summing up the contributions from the whole velocity space one obtains the expected number of helium atoms measured by the detector for the pixel (ϵ_i, α_j):

$$Z_{ij}^{\mathrm{He}} = T_{\mathrm{I}}\, S \int_{\alpha_j - 1/2\Delta\alpha}^{\alpha_j + 1/2\Delta\alpha} \mathrm{d}\alpha \int G(\theta)\, f_{\mathrm{eff}}(E_{\mathrm{rel}})\, v_{\mathrm{rel}}\, F(\mathbf{v};\mathbf{r})\, \mathrm{d}^3 v \tag{2}$$

The first integral corresponds to the smearing effect, while the second one takes into account all allowed velocity vectors at $\mathbf{r}$, i.e. speeds equal to and greater than the parabolic velocity at this point. The integration over velocity is practically limited to those directions for which $G(\theta)$ is non-zero ($\theta < \theta_{\max}$). The inner integral in (2) is written in the ecliptic coordinate system. However since the function $G(\theta)$ and the limits of integration are most naturally defined in the spacecraft coordinate system, formula (2) will be later transformed into the Ulysses s/c frame (Sect. 4.2).

In addition to the signal from helium atoms (2) there are two other contributions to the observed counts Z_{ij}. The first contribution is comprised of dark counts such as cosmic rays, EUV photons, etc., and is accounted for by the background Z_{ij}^{bckg}. The second possible contribution Z_{ij}^{heavy} comes from neutral atoms heavier than helium, like oxygen and neon (Sect. 4.6). Then the total count numbers can be given as:

$$Z_{ij} = Z_{ij}^{\mathrm{He}} + Z_{ij}^{\mathrm{heavy}} + Z_{ij}^{\mathrm{bckg}} \tag{3}$$

which can be directly compared with the observations (Sect. 4.).

Observations as well as theoretical considerations suggest that the distribution function of neutrals in the LISM should be Maxwellian (or well approximated by a Maxwellian) (Meier 1977; Wu & Judge 1979). In the first attempt to determine the helium parameters for the LISM we therefore assume a Maxwellian for the particle distribution at infinity; however, in a later stage, with a sufficiently accurate data base, it should be possible to test this assumption.

3. Inverse method

Generally, inverse methods and related observational techniques are used when one seeks to obtain quantitative information about a source function (cause) of some physical process from measurements of a response function (effect). Typical applications include tomography, seismology, remote sensing of planetary and stellar atmospheres, image processing, etc. (Tarantola 1987; Parker 1977; Craig & Brown 1986). Inverse problems are always more complicated and demand more computational power than direct problems, where the effect is calculated from the cause; they are closely related to integral equations (Press et al. 1992).

In many cases inverse methods are applied when a large number of unknown parameters is to be determined from an equally large, or smaller set of measurements (Press et al. 1992). Then, necessarily, the problem is ill-conditioned and requires sophisticated techniques to find the best solution. Usually, the trick is to apply a regularization method. It replaces the original problem by a well-determined alternative by using additional information or constraints on the parameters. In our case, fortunately, the number of unknowns – the five parameters of the Maxwellian distribution at infinity: three velocity components, density, and temperature, is small as compared with the number of pixels with measured counts. This does not rule out the possibility that the problem is singular (ill-conditioned) and a unique solution cannot be found without regularization. Therefore, we will generally keep a regularization term in our considerations, but make it negligibly small if the problem is well-conditioned.

We have chosen Tarantola's approach, which is extensively used in seismology, to solve our inverse problem (Tarantola 1987). First simulations showed that this method is well suited to determine the distribution function at infinity from the data at 1 AU (Banaszkiewicz et al. 1990). The philosophy of Tarantola in dealing with inverse problems is a probabilistic interpretation of all factors involved. The basic relation between the measured quantities represented by a N-dimensional vector $\mathbf{y}$, and model parameters described by a M-dimensional vector $\mathbf{x}$ reads:

$$\mathbf{y} = \mathbf{g}(\mathbf{x}) \tag{4}$$

where $\mathbf{g}(\mathbf{x})$ is, in general, a non-linear function. In this relation $\mathbf{y}$ is the result of 'ideal' measurements for given $\mathbf{x}$ or, in other words, the value predicted for the input set of parameters $\mathbf{x}$ according to our best possible knowledge of underlying physics and instrumental effects. In reality, however, we neither know exactly the input parameters nor obtain accurately the measured values. Therefore, it seems natural to describe all these uncertainties in terms of probability densities: $\tilde{\rho}_{\mathrm{D}}(\mathbf{y};\mathbf{y}_{\mathrm{obs}})$ – the a priori probability density that the true value of measured quantities is $\mathbf{y}$, if the value registered by the instrument is $\mathbf{y}_{\mathrm{obs}}$; $\rho_{\mathrm{M}}(\mathbf{x};\mathbf{x}_{\mathrm{prior}})$ – the a priori probability density that the true value of the input parameters is $\mathbf{x}$ for the given reference value $\mathbf{x}_{\mathrm{prior}}$ which usually corresponds to the best known value so far; $\Theta(\mathbf{y}|\mathbf{x})$ – the conditional probability density that one gets the measured value $\mathbf{y}$ for the input parameters $\mathbf{x}$. The last function represents uncertainties in the fundamental relation (3). The a posteriori probability density $\sigma_{\mathrm{M}}(\mathbf{x})$ for the input parameters can then be calculated according to Bayes' theorem:

$$\sigma_{\mathrm{M}}(\mathbf{x}) = \rho_{\mathrm{M}}(\mathbf{x};\mathbf{x}_{\mathrm{prior}}) \times \int \tilde{\rho}_{\mathrm{D}}(\mathbf{y};\mathbf{y}_{\mathrm{obs}})\, \Theta(\mathbf{y}|\mathbf{x})\, \mathrm{d}\mathbf{y} \tag{5}$$

Following Tarantola (1987), we assume that all probability densities on the RHS of (4) are Gaussian (which is quite

obvious for $\tilde{\rho}_{\rm D}(\mathbf{y};\mathbf{y}_{\rm obs})$, but not so evident for the other two densities):

$$\tilde{\rho}_{\rm D}(\mathbf{y};\mathbf{y}_{\rm obs}) = (2\pi^N \det\mathbf{C_y})^{-1/2} \times \exp\left(-\frac{1}{2}(\mathbf{y}-\mathbf{y}_{\rm obs})^{\rm T}\mathbf{C_y}^{-1}(\mathbf{y}-\mathbf{y}_{\rm obs})\right) \quad (6)$$

$$\rho_{\rm M}(\mathbf{x};\mathbf{x}_{\rm prior}) = (2\pi^M \det\mathbf{C_x})^{-1/2} \times \exp\left(-\frac{1}{2}(\mathbf{x}-\mathbf{x}_{\rm prior})^{\rm T}\mathbf{C_x}^{-1}(\mathbf{x}-\mathbf{x}_{\rm prior})\right) \quad (7)$$

$$\Theta(\mathbf{y}|\mathbf{x}) = (2\pi^N \det\mathbf{C_g})^{-1/2} \times \exp\left(-\frac{1}{2}(\mathbf{g}(\mathbf{x})-\mathbf{y})^{\rm T}\mathbf{C_g}^{-1}(\mathbf{g}(\mathbf{x})-\mathbf{y})\right) \quad (8)$$

where $\mathbf{C_y}$, $\mathbf{C_x}$, and $\mathbf{C_g}$ are the covariance matrices. Substituting (6), (7), and (8) into (5) one obtains:

$$\sigma_{\rm M}(\mathbf{x}) \propto \exp\left(-\frac{1}{2}(\mathbf{g}(\mathbf{x})-\mathbf{y}_{\rm obs})^{\rm T}\mathbf{C_{gy}}^{-1}(\mathbf{g}(\mathbf{x})-\mathbf{y}_{\rm obs}) - \frac{1}{2}(\mathbf{x}-\mathbf{x}_{\rm prior})^{\rm T}\mathbf{C_x}^{-1}(\mathbf{x}-\mathbf{x}_{\rm prior})\right) \quad (9)$$

with $\mathbf{C_{gy}} = \mathbf{C_g} + \mathbf{C_y}$.

The set of parameters $\mathbf{x}$ which describes the measurements in the best way corresponds to the maximum of the probability density $\sigma_{\rm M}(\mathbf{x})$ or, equivalently, to the minimum of the function:

$$S(\mathbf{x}) = \frac{1}{2}(\mathbf{g}(\mathbf{x})-\mathbf{y}_{\rm obs})^{\rm T}\mathbf{C_{gy}}^{-1}(\mathbf{g}(\mathbf{x})-\mathbf{y}_{\rm obs}) + \frac{1}{2}(\mathbf{x}-\mathbf{x}_{\rm prior})^{\rm T}\mathbf{C_x}^{-1}(\mathbf{x}-\mathbf{x}_{\rm prior}) \quad (10)$$

Applying these general expressions to the problem of interstellar neutral helium one finds that the data vector corresponds to the measured counts $y_{ij} \equiv Z_{ij}$, $i = 1,\ldots,I; j = 1,\ldots,J$; $N = I \cdot J$, the model parameters are normalized to some reference values (usually corresponding to the best literature values) for the helium density, the bulk velocity and the temperature of the LISM $\mathbf{x} = (n_\infty/n_{r,\infty}, v_{{\rm b},x;\infty}/v_{{\rm b},x;r,\infty}, v_{{\rm b},y;\infty}/v_{{\rm b};r,\infty}, v_{{\rm b},z;\infty}/v_{{\rm b},z;r,\infty}, T_\infty/T_{r,\infty})$, and relation (4) is, in our specific problem, equivalent to formulae (3) and (2).

The first term in the minimized function $S(\mathbf{x})$ is equal to a sum of squares of weighted residuals – or equivalent to χ^2 (Meyer 1975). The second term constrains the values of the parameters to be determined – they should be as close as possible to the reference (a priori) values $\mathbf{x}_{\rm prior}$. The relative importance of these two terms depends on the covariance matrices $\mathbf{C_{gy}}$ and $\mathbf{C_x}$. We will assume that the data as well as the parameters are, a priori, not, i.e. the covariance matrices $\mathbf{C_{gy}}$ and $\mathbf{C_x}$ are diagonal. If the count numbers are random variables distributed according to Poisson statistics then the diagonal terms in the data covariance matrices should scale as the count numbers themselves, provided that $|\mathbf{C_g}| \ll |\mathbf{C_y}|$. The latter holds if our assumptions of a Maxwellian distribution at infinity and on the transport processes are correct.

We can evaluate the optimization quality by a goodness-of-fit probability $Q(\chi^2 \geq \chi^2_{\rm bf})$, where $\chi^2_{\rm bf}$ is calculated for the best fit parameters. If the value Q smaller than the confidence level $Q_{\rm cl}$, then the obtained parameters are not statistically reliable. Usually the $Q_{\rm cl}$ value is set as 0.05 or 0.1 , but in many instances even much smaller values are accepted (Press et al. 1992; Meyer 1975).

More difficult to deal with is the error determination. If this were a linear problem, the covariance matrix could be obtained easily from the design matrix (Meyer 1975). In the case of a nonlinear problem we first have to linearize $Z_{ij}(\mathbf{x}) \approx Z_{ij}(\mathbf{x}^{(0)}) + (\delta Z_{ij}/\delta x_k)(\mathbf{x}^{(0)})\Delta x_k$ and then calculate the variance of parameters $\sigma^2_{x_i} = \mathbf{C_{x;ii}}$ from the a posteriori covariance matrix.

Among the different methods for obtaining the minimum of $S(\mathbf{x})$ we prefer the optimization technique, since it is robust and guarantees that a solution will be found. We have tried a few algorithms; at first, the three methods described by Press et al. (1992). All of them give similar results, but the simplest one - the Powell method - is also the fastest one. The common disadvantage of these algorithms is that they are unconstrained, i.e. they try to find the solution in the whole $\mathbf{x}$-space of parameters, which is ineffective (trials with temperatures $T = 100000$ K, for example, are meaningless) and may lead to numerical difficulties (negative density and temperature). We avoid these difficulties by: (i) changing the variables to $\log T$ and $\log n$, and (ii) introducing a cost function which increases the value of $S(\mathbf{x})$ in the unlikely (from the point of view of physics) regions of the $\mathbf{x}$-space. Finally, the NAG-library routine E04UPF (NAG Mark 15 1993) was used which finds a minimum of a sum-of-squares function for a general, constrained optimization problem.

4. Application to actual measurements

With the knowledge of the previously determined LISM characteristics and the experience gained from processing many GAS-ULYSSES data sets we put the following (liberal) limits on the acceptable range of helium parameters at infinity: $0.003 \leq n_\infty \leq 0.06\ {\rm cm}^{-3}$, $4.0 \leq v_{{\rm b},x;\infty} \leq 12.0$ km/s, $15.0 \leq v_{{\rm b},y;\infty} \leq 33.0$ km/s, $-5.0 \leq v_{{\rm b},z;\infty} \leq +3.0$ km/s, and $3000 \leq T_\infty \leq 12000$ K. Since the optimization routine calls the user-supplied function many times that calculates count rates according to formula (1), as four-fold integrals, it is important to organize the program in the most efficient way. For typical data sets of 100

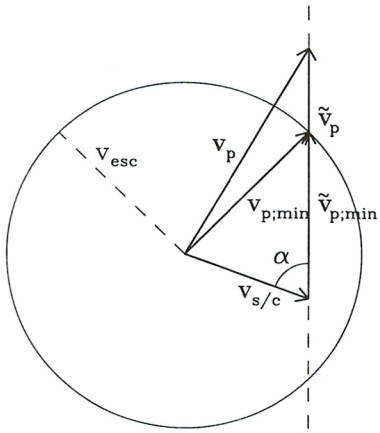

Fig. 4. The apparent velocity vectors $\tilde{\mathbf{v}}_p$ of neutral particles as observed at the spacecraft for a given direction (dashed line). They are differences of the spacecraft velocity $\mathbf{v}_{s/c}$ and the actual particle's velocity $\mathbf{v}_p$ in the ecliptic coordinate system. The minimum velocity $\tilde{\mathbf{v}}_{p;min}$ corresponds to the local escape velocity $\mathbf{v}_{esc}$ in the ecliptic coordinate system

pixels and 50-100 iterations in the optimization routine up to 10000 computations of Z_{ij} are required.

Yet another problem is introduced by the variations of the elevation and azimuth grid steps $\Delta\epsilon$ and $\Delta\alpha$ from one data set to the next. At the beginning of the mission, with $\Delta\alpha = 11.^\circ 2$, these steps are of the order of the angular width of the helium distribution (half-width at half-maximum); later, with typically $\Delta\alpha = 2.^\circ 8$, they are much smaller. To cope with this difficulty we have introduced a computational grid with prescribed steps in elevation and azimuth (usually $\Delta\epsilon_c = 2°$, and $\Delta\alpha_c = 4°$). This grid covers an area slightly larger than the area of the processed subimage. All quantities which do not depend on the x-parameters (e.g. navigational data) are first calculated on the computational grid.

Especially important is the determination of a set of particle orbits which link the point of observation with infinity. The parameters of these trajectories are stored for later use in the optimization loop.

In summary, the organization of the program is as follows:

- a sub-image containing 30-120 pixels centered around the neutral helium signal is chosen from the whole image with 32 azimuthal steps and 10-20 elevation steps,
- the background value Z^{bckg} is determined,
- variables which do not depend on $\mathbf{x}$ are calculated
- the optimization routine is called until the best values of $\mathbf{x}$ are found.

We will now briefly summarize the most important points of the algorithm to calculate the simulated count rates Z_{ij} according to relations (2) and (3).

4.1. *Input data sets*

For each observation of the interstellar helium flux all necessary information is provided in two data files. The first one contains:

(i) the measured counts from two detectors in form of a 2D array of pixels with 32 columns (azimuth) and a variable number of rows (10-20 elevation steps), and the values of azimuth and elevation for all grid points (pixels) – see e.g. Figs. 5 and 7, upper panels;
(ii) the integration time for each grid point;
(iii) counts per second calculated from (i) and (ii);
(iv) universal times of the beginning and the end of the interval of observation and for the beginning of each elevation step.

The second file contains navigational data: the spacecraft position and velocity as well as the spin axis orientation of Ulysses in the ecliptic coordinate system for the beginning, the centre, and the end of the observational interval.

4.2. *Coordinate systems and velocity transformation*

The relationship between the relevant coordinate systems, the solar ecliptic and the spacecraft coordinate systems is indicated in Fig. 2. The spin axis $z_{s/c}$ points towards Earth, the $-y_{s/c}/z_{s/c}$ quadrant contains the Sun by definition. In the s/c-coordinate system the pointing direction of the detector is given in spherical coordinates: azimuth α and elevation ϵ. The transformation matrix $\mathbf{T}$ between the two c.s. is determined for each time interval corresponding to a single elevation scan, for a given spin axis orientation and spacecraft position $\mathbf{r}_{s/c}$. These data as well as the spacecraft velocity $\mathbf{v}_{s/c}$ are interpolated from the navigational data provided in the second input data file. The neutral particle velocity in the spacecraft c.s. $\tilde{\mathbf{v}}$ is related to its local velocity in the ecliptic c.s $\mathbf{v}$ through the transformation (Fig. 4):

$$\tilde{\mathbf{v}} = \mathbf{T}\,(\mathbf{v} - \mathbf{v}_{s/c}) \tag{11}$$

4.3. *Calculation of the local distribution function*

As indicated in the introduction, the local distribution function $F(\mathbf{r}, \mathbf{v};\ n_\infty, \mathbf{v}_\infty, T_\infty)$ at the position $\mathbf{r}$ of the observer is derived from the Maxwellian distribution function at infinity $F(\mathbf{v})$ for a particle with mass m:

$$F(\mathbf{v};\ n_\infty, \mathbf{v}_\infty, T_\infty) = n_\infty \left(\frac{m}{2\pi k T_\infty}\right)^{3/2} \times \exp\left(-\frac{m(\mathbf{v}_\infty - \mathbf{v}_{b;\infty})^2}{2kT_\infty}\right), \tag{12}$$

by applying Liouville's theorem. As we can assume Keplerian orbits, the calculation of the local velocity vector is elementary (Fahr 1971). Deflection due to radiation pressure can be neglected for neutral helium. Furthermore,

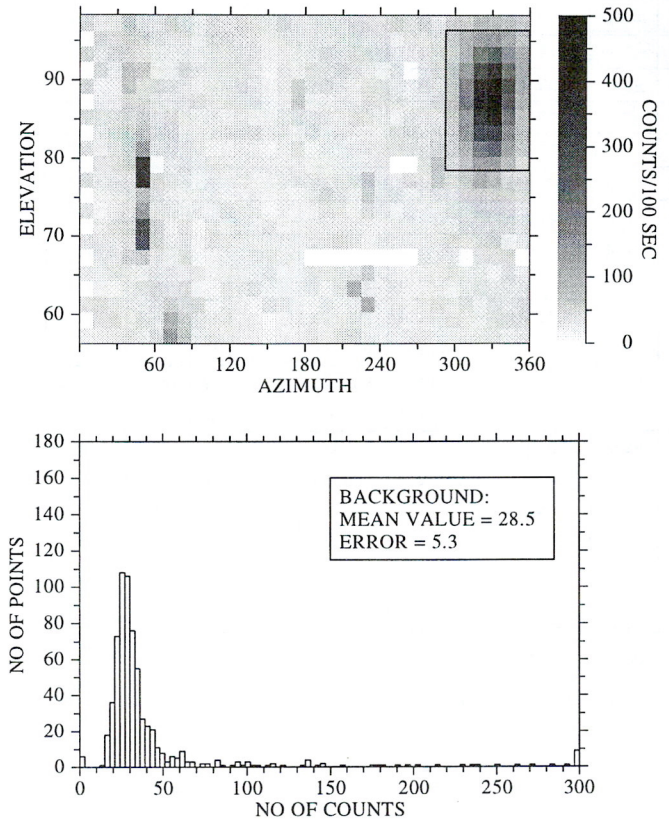

Fig. 5. Upper part: the full image (counts/100 s) and the sub-image (inside the rectangle) with the signal from helium atoms for the data set 3610.2B. Lower part: the histogram of count numbers used to determine the background level. Note, that the bright pixels from UV-star light are excluded from further analysis by choosing a proper sub-image

loss processes due to charge exchange with solar wind α-particles do not play a role because of the negligibly small cross-sections involved. However, the fraction of particles which survive against photoionization loss is included according to the classical formula (Wu & Judge 1980; Fahr 1971):

$$L = \exp(-\frac{\beta_{\rm ion} r_{\rm e}^2}{h}\vartheta), \tag{13}$$

where ϑ is the angular deflection of the particle's trajectory from infinity to the observer's position $\mathbf{r}$, $r_{\rm e} = 1$ AU, and $\beta_{\rm ion}$ is the ionization rate (at 1 AU).

4.4. *Count number calculations*

We transform relation (1) into the spacecraft coordinate system. The transformation matrix $\mathbf{T}$ in (11) is orthogonal, therefore $\mathrm{d}^3\tilde{\mathbf{v}} = \mathrm{d}^3\mathbf{v}$. It is convenient to introduce spherical coordinates with the polar axis aligned with the optical axis of the instrument. In this frame formula (2) reads:

$$Z_{ij} = T_{\rm I}\, S \int_{\alpha_j - 1/2\Delta\alpha}^{\alpha_j + 1/2\Delta\alpha} \mathrm{d}\alpha \int_0^{2\pi} \int_{\cos\theta_{\max}}^{1} G(\theta)\, \mathrm{d}\varphi\, \mathrm{d}\cos\theta \times \int_{v_{\min}}^{v_{\max}} f_{\rm eff}(E_{\rm rel})\, v_{\rm rel}\, F(\mathbf{v};\mathbf{r})\, \mathrm{d}\tilde{v}. \tag{14}$$

The limits of the innermost integral over speed are set to differ by about $\pm 8 - 10$ km/s from the bulk helium speed in the s/c-coordinate system. The integration over v is performed by the trapezoid method on a grid of 12 or 24 points. The accuracy is better than 1% and was checked by comparing the results for $K = 12, 24$ grid points with those for $K = 96$.

The integration over angles with the geometry function $G(\theta)$ (Fig. 3) is performed with a parallelepiped method (2D trapezoid) on a grid of 61 points (the central point and 5 rings centered at the optical axis with 12 equidistant points in each ring). To estimate the accuracy of this integration we compared the value of the angular field-of-view (in steradians) obtained analytically with the integral. They differ by less than 1.5% for NFOV and by less than 1% for WFOV.

Finally, in cases where the resolution in azimuth angle ($\Delta\alpha = 11\overset{\circ}{.}2$) is only of the order of the width of the angular distribution and the FOV moves in this angular bin as the spacecraft rotates (smearing effect), the temperature determination depends on the method of interpolation between neighboring pixels. A 3-point (parabolic) interpolation is used, as a simple linear interpolation leads to temperatures higher by $\approx 500-800$ K.

The variation of statistical significance due to different integration times T_{ij} was taken into account by introducing a weight $\sigma_{ij}^2 = Z_{ij}(T_{100}/T_{ij})^2$, where $T_{100} = 100$ s is our standard normalization time.

4.5. *Background determination and sub-image definition*

In general, a dataset (image) contains an angular range (sub-image), in which the helium particles are registerd. The area outside that range is used to determine the omnidirectional background which is also contained in the sub-image (Figs. 5 and 7). A precise determination of the background is required as an error in the background directly transforms into an error in the helium density and temperature determination. In principle, the background $Z^{\rm bckg}$ for the assumed Poisson distribution of the count numbers Z_k in the K background pixels would be (Meyer 1975):

$$Z^{\rm bckg} = \frac{1}{K}\sum_{k=1}^{K} Z_k. \tag{15}$$

Table 1. Results

no	Data sets	Method[2]	NP[3]	T_∞[1]	ΔT_∞	v_∞	Δv_∞	β_∞	$\Delta\beta_\infty$	λ_∞	$\Delta\lambda_\infty$	n_∞	Δn_∞	Residuum[4]	χ^2	Q[5]
1	3610.2A	c	54	7063	±2993	25.13	±2.08	-4.72	±1.89	73.31	±4.88	0.0181	±0.0034	1.00	48.9	0.48
2	3610.2B	c	54	7396	±3132	25.06	±1.89	-5.37	±1.83	73.95	±4.52	0.0130	±0.0023	0.96	45.0	0.64
3	2871.1A	a	99	5369		25.54		-5.33		73.83		0.0196		1.15	123.5	0.17E-1
4	2871.1B	a	99	6360		25.13		-4.79		74.77		0.0227		1.14	122.4	0.28E-1
5	2871.1A	b	99	5447	±23600	25.52	±66.0	-4.75	±3.80	73.74	±94.0	0.0195	±0.47	1.16	127.8	0.13E-1
6	2871.1B	b	99	6499	±27400	25.78	±65.38	-5.03	±3.43	74.31	±91.7	0.0218	±0.159	1.15	126.1	0.22E-1
7	3610.2A	c	54	6300	±2186	24.79	±1.77	-4.63	±1.59	74.47	±3.89	0.0175	±0.0038	1.05	190.9	0.87E-2
	2871.1A		99									0.0216	±0.0109	1.21		
8	3610.2B	c	54	6387	±2068	24.53	±1.52	-4.89	±1.44	75.71	±3.33	0.0124	±0.0022	1.15	198.7	0.34E-2
	2871.1B		99									0.0250	±0.0106	1.19		
9	3610.2A	c	54	7302	±2192	25.07	±1.39	-5.21	±1.33	73.80	±3.30	0.0183	±0.0032	1.07	104.1	0.42
	3610.2B		54									0.0129	±0.0021	1.00		
10	2871.1A	c	99	6382	±20100	25.99	±49.3	-5.38	±2.54	73.91	±68.1	0.0197	±0.107	1.18	280.7	0.44E-3
	2871.1B		99									0.0210	±0.114	1.20		
11	3610.2A	c	54	6341	±1499	24.58	±1.13	-4.82	±1.07	75.47	±2.50	0.0175	±0.0030	1.15	401.6	0.57E-4
	2871.1A		99									0.0231	±0.0102	1.21		
	3610.2B		54									0.0124	±0.0020	1.15		
	2871.1B		99									0.0246	±0.0093	1.21		

[1] Units: temperature T_∞: K, bulk speed v_∞: km/s, direction of the bulk velocity β_∞, λ_∞: °, density n_∞: cm^{-3}.

[2] a – simple; the solution on the line of equal residuals is found as the closest to the reference solution
b – semiautomatic; the second term in (10) effectively constrains the velocity values to be as close as possible to the reference values
c – automatic; unconstrained optimization with the negligible second term in (10)

[3] number of pixels in the subimage

[4] in units of (χ^2) - expected value of χ^2-function

[5] goodness-of-fit value (see Section 3)

However, in the case of GAS data some addditional factors have to be taken into account: (i) The background value might not be constant across the image; one of the important background sources is scattered Ly-α, which is not isotropic. It is enhanced in the upwind direction. The corresponding asymmetry, of the order of a few counts/100 s, can be seen in some data sets. (ii) zero counts can sometimes result from instrumental effects or from gaps in data transmission. (iii) UV-light from stars can contaminate the set of background pixels. Bright stars can be identified and eliminated, fainter ones which add a few counts to the background are impossible to trace. However, as these stars are concentrated along the Milky Way. Depending on the position of the spacecraft, this is a problem only in a few cases. (iv) The integration times for pixels from the same data set may differ due to operational conditions (e.g. available telemetry rate). As the actual integration time is known, this is taken into account by a special weighting function in the analysis of the Poisson distribution.

Only the pixels in the so called sub-image (see Figs. 5 and 7) are used in the helium parameter determination. Because of the above mentioned uncertainties in the background it is reasonable to tailor the sub-image that it does not include too many pixels with values close to Z^{bckg}. On the other hand a quite extended sub-image is required to accurately determine the temperature. As a compromise we usually chose a rectangular sub-image with 30–120 pixels with count numbers in the boundary pixels 1.5–2 times larger than the background value.

4.6. *Contribution from heavy neutrals*

Using the cosmic abundance of oxygen and neon (Fahr 1990) together with appropriate ionization rates, we have simulated the contribution of these species to the observed He-distributions. Although their distribution in velocity space is narrower than that of helium at the same temperature, it turned out that their contribution to the count rates in the center of the distribution is only 5% and thus of the same order as the statistical fluctuations. Hence a reliable determination of these particles would not be possible. These count rates, however, are taken into account in the model, to improve the determination of the helium parameters. The densities used, are 8 10^{-5} cm^{-3} for oxygen and 2 10^{-5} cm^{-3} for neon, and ionization rates 9 10^{-7} s^{-1} and 2 10^{-7} s^{-1}, respectively (Fahr 1990).

5. Examples

After describing the theoretical considerations, we shall now demonstrate the power and the limitations of this

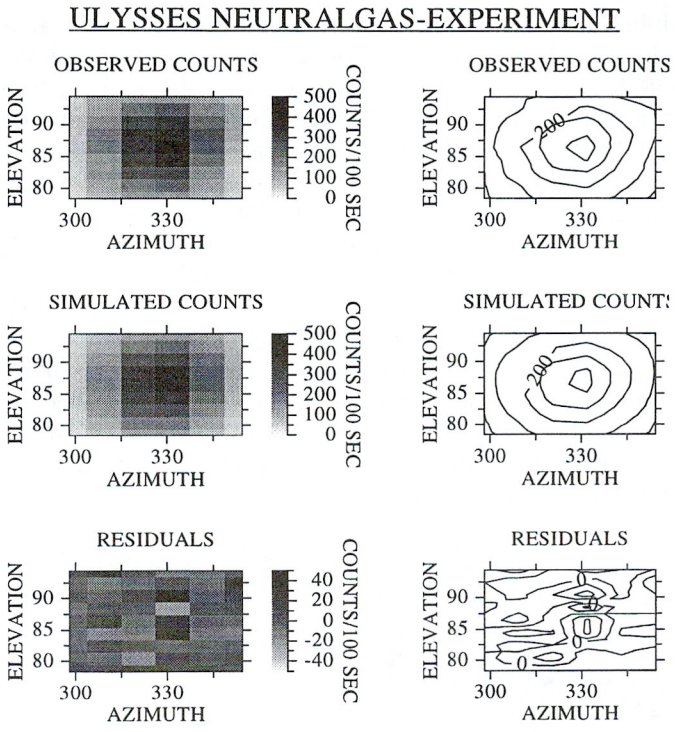

Fig. 6. The observed, simulated, and residual (observed minus simulated) count numbers for the sub-image in Fig. 5. The simulated counts are obtained for the best fit helium parameters that are determined by minimizing the sum of squared residuals

method by analysing in detail two extreme, but still typical, cases. The results, error estimates, confidence level, etc., are summarized in Table 1. In both cases we have simultaneous data from the two telescopes A and B, with the narrow field of view (NFOV) and wide field of view (WFOV), respectively. However, to show the principle, in many cases we shall refer only to the data from telescope B.

5.1. *Observational conditions*

The first data set (Fig. 5), coded as 3610.2, was obtained on Dec. 28, 1990 at the Ulysses position $\mathbf{r} = (-0.18, 1.53, 0.05)$ AU (in heliocentric ecliptic coordinates), which corresponds to a heliocentric distance of about 1.55 AU – downwind and still just in the helium cone. The second data set, named 2871.1 (Fig. 7) was taken on Sept. 14, 1991, when Ulysses was at a distance of about 4.45 AU ($\mathbf{r} = (-3.89, 2.15, 0.10)$ AU), essentially crosswind to the general helium flow. In the first case, from the whole image (672 pixels of $\Delta\alpha = 11\overset{\circ}{.}2$ and $\Delta\epsilon = 2°$) a sub-image of 9 elevation × 6 azimuth grid points was chosen (Fig. 5, upper panel). Similarly, in the second case (Fig. 7, upper panel) a sub-image of 11 × 9 pixels ($\Delta\alpha = 2\overset{\circ}{.}8$ and $\Delta\epsilon = 2°$) was selected, to separate pixels containing helium from the general background. In the area outside the sub-image the background was determined from the Poisson distribution (Figs. 5 and 7, lower panels) to be 28.48 cts/100 s (WFOV) and 15.58 cts/100 s (NFOV) in the first case and 33.99 and 18.15, respectively, in the second case.

In December 1990 the spacecraft velocity was relatively high ($\approx$ 33 km/s) with an angle of about 40° to the local flow of neutral atoms. As a result, a relative velocity of the particles in the instruments frame of reference of about 65 km/s (corresponding to a relative energy of about 90 eV) provided a large detector efficiency ($\approx 1.5\ 10^{-2}$; see Fig. 1), and, in consequence, a high count number. In addition the neutral flux at the detector was still enhanced due to the focusing effect of the Sun's gravity. The observational conditions were less favorable in September 1991, when the spacecraft velocity was about 18 km/s and the neutrals flowed from an angle of 45° with respect to the neutral flow. This resulted in a relative velocity of 45 km/s (42 eV) and a lower efficiency. The statistical noise amounts to 3% (3610.2B) and 9% (2871.1B) for the maximum. For the further analysis, in both cases the ionization rate was assumed to be $1.4 - 1.5\ 10^{-7}$ s^{-1} in the end of 1990 - shortly after the maximum of solar activity; it could be slightly less nine months later, when 2871.1 data set was taken (Fahr 1990).

5.2. *Unconstrained optimization*

As a first attempt in the helium parameter determination, we performed a minimization of $S(\mathbf{x})$ with diagonal elements of $C_\mathbf{x}$ equal to 10 (note that $\mathbf{x}$ are the normalized helium parameters and, therefore, they are usually of the order of 1). Hence, the second term in (10) was very small (0.01%) in comparison with the sum of squared residuals and the optimization was practically not constrained by the choice of $\mathbf{x}_{\rm prior}$. We have found well-determined minima for both 3600.2 data sets which correspond to the following sets of helium parameters (for $\beta_{\rm ion} = 1.4\ 10^{-7}$ s^{-1}): $T_\infty = 7064$ K, $v_\infty = 25.13$ km/s, $\beta_\infty = -4\overset{\circ}{.}72, \lambda_\infty = 73\overset{\circ}{.}31, n_\infty = 0.018$ cm^{-3}, for NFOV, and $T_\infty = 7396$ K, $v_\infty = 25.06$ km/s, $\beta_\infty = -5\overset{\circ}{.}37, \lambda_\infty = 73\overset{\circ}{.}95, n_\infty = 0.013$ cm^{-3}, for WFOV (Fig. 6). The bulk velocity of helium atoms at infinity $\mathbf{v}_{\rm b;\infty}$ is given in spherical coordinates, i.e. in terms of modulus v_∞, ecliptic latitude β_∞, and ecliptic longitude λ_∞.

However, for the second data set no unique, distinct minimum could be found - the problem is ill-conditioned. There is, instead, a line of almost constant $S(\mathbf{x})$ in the five dimensional parameter space. The variation of $S(\mathbf{x})$ along this line is less than 1%, i.e. much smaller than the

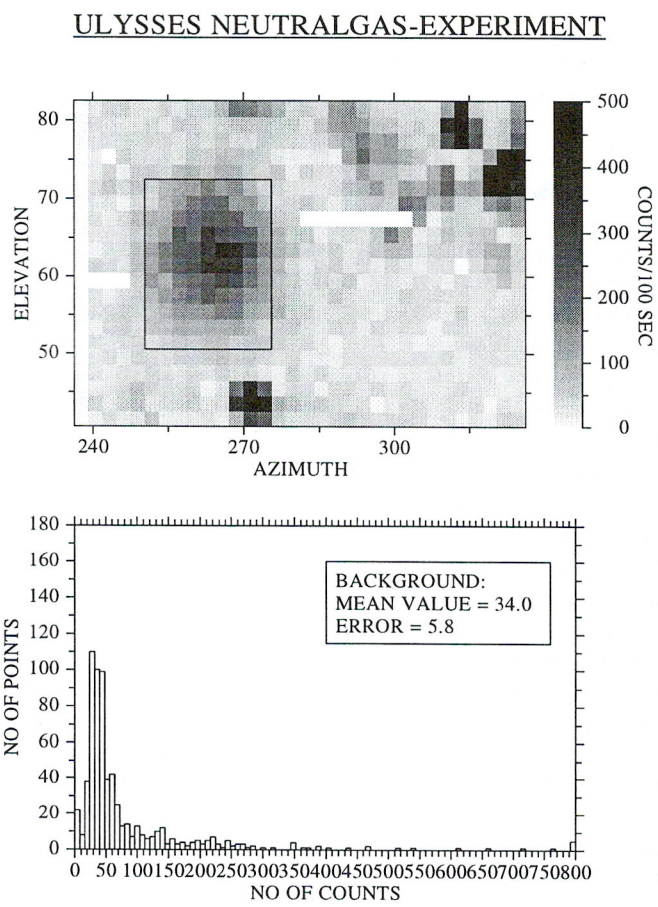

Fig. 7. The same plots as in Fig. 5, but for the data set 2871.1B

estimated error of the helium parameters (see Sect. 5.4). This line can be parametrized by any of the input parameters, for example, $v_{x;\infty}$. Assuming a reference value $v_{x;\infty} = 7$ km/s (which is close to the optimum of the first case) with a variation of ± 1 km/s we obtain for the WFOV (for $\beta_{\rm ion} = 1.4\ 10^{-7}\ {\rm s}^{-1}$):
$T_\infty = 6521. \pm 475$ K, $v_\infty = 25.83 \pm 1.14$ km/s $\beta_\infty = -4\overset{\circ}{.}80 \mp 0\overset{\circ}{.}022$, $\lambda_\infty = 74\overset{\circ}{.}22 \mp 1\overset{\circ}{.}60$, $n_\infty = 0.0217 \mp 0.00295\ {\rm cm}^{-3}$. Simulated counts and residuals for one of the possible solutions are shown in Fig. 8. In the case of the NFOV the obtained values and variations are similar, with the exception of the temperature and density, which are equal 5340 K and 0.0198 cm^{-3}, respectively.

It is not immediately obvious why in one case a well-determined minimum exists, and not in the other one. To study the difference between the two cases (3601.2 and 2871.1) in more detail we have analyzed the most important factors that determine the values of the simulated count numbers Z_{ij}. In the first approximation we can neglect smearing and replace the integration over angles in (14) by multiplication by $\Delta\Omega$ - the effective solid angle of the GAS-instrument field-of-view. We have calculated all the factors which enter the integrand I_v in the remaining integral over speed. Clearly, the variation of the distribution function F dominates the other factors. Only for the 2871.1 data set, the efficiency function $f_{\rm eff}$ plays a substantial role in shaping the integrand. Each combination of direction (ϵ_i, α_j) and speed $\tilde{v}$ corresponds to a unique particle velocity at infinity $\mathbf{v}_\infty$. The variation of $\tilde{v}$ within the limits of integration can, therefore, be mapped into a section of a curve in a velocity space at infinity: $\mathbf{v}_{\infty;ij}(\tilde{v})$ (Figs. 9, 10). This line intersects the distribution function at different distances from its center (bulk velocity of neutrals). The contribution to the integral is the largest at a point $P_{\rm m}$ where the distance is the smallest. This point corresponds to the maximum of the function I_v. Since the thermal velocity of helium is only about 6-7 km/s, the significant contribution to the integral comes from a well localized region around the maximum.

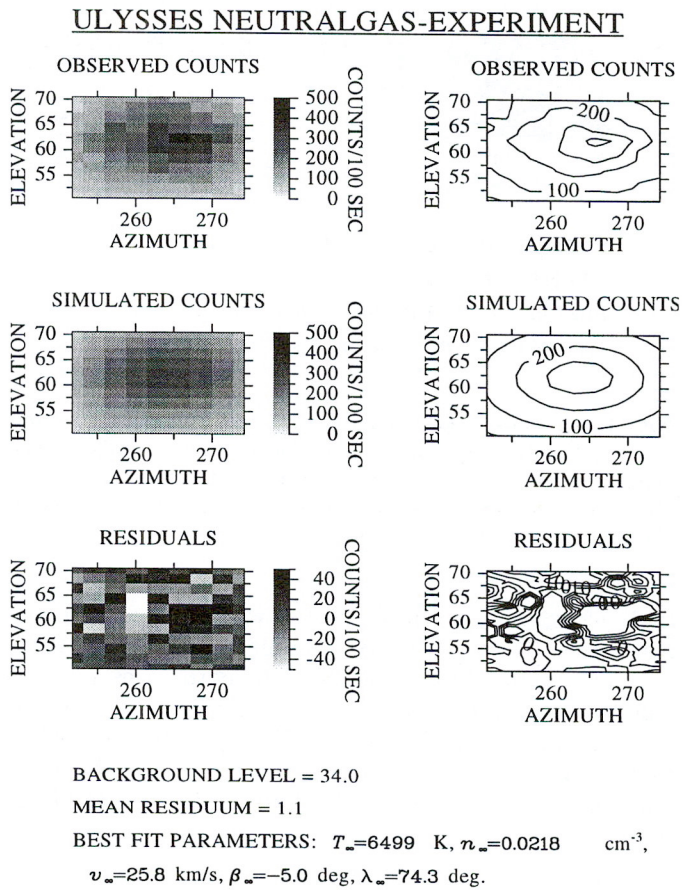

Fig. 8. The same plots as in Fig. 6, but for the data set 2871.1B

Let us consider now a family of lines $\mathbf{v}_{\infty;ij}(\tilde{v})$; $i = 1, \ldots, I$; $j = 1, \ldots, J$ that correspond to different directions (ij) (Figs. 9, 10). Their locations in velocity space do not depend on the parameters of the distribution function, but the positions of $P_{\rm m}$ do. The only possibility of obtaining the same value of the speed integral for two (or more) different sets of He parameters is to preserve the

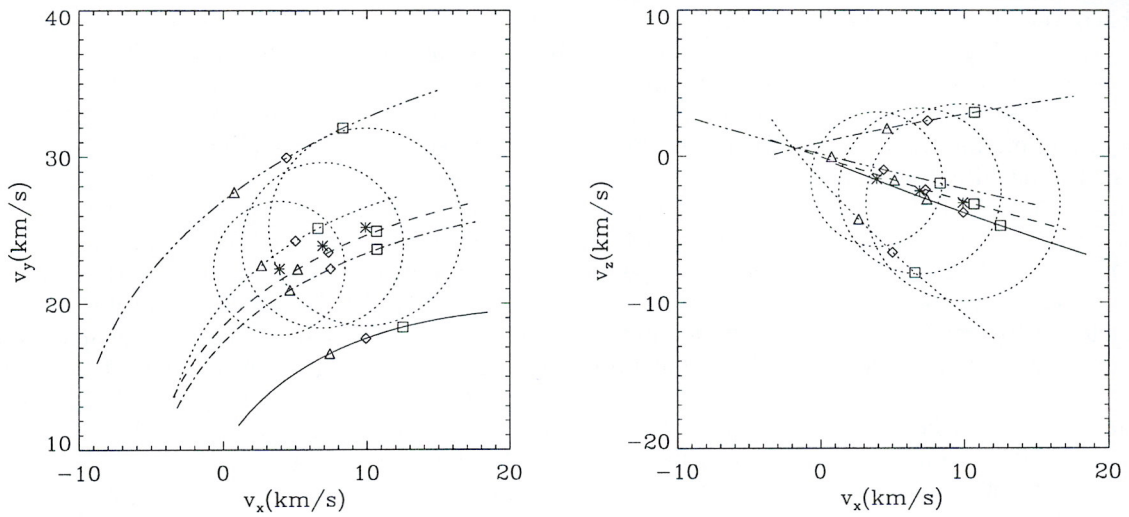

Fig. 9. Data set 3610.2B. Each line contains loci of the particle velocities at infinity for a given viewing direction of the instrument (representing the directions of the pixel with the maximum counts and its neighbouring pixels in Figs. 5, 7, upper panels): ($\epsilon = 78°, \alpha = 328°$) – solid line, ($\epsilon = 86°, \alpha = 312°$) – dotted line, ($\epsilon = 86°, \alpha = 328°$) – dashed line, ($\epsilon = 86°, \alpha = 344°$) – dashed-dotted line, and ($\epsilon = 94°, \alpha = 328°$) – dashed-triple_dotted line. For each line, points $P_{\rm m}$ corresponding to the maximum contributions to $I_v(\tilde{v})$ are marked by different symbols for three helium bulk velocities found as the best fit parameters in the constrained optimization problem (a constraint $v_{x;\infty} = \text{const}$ has been applied in each case): ($\triangle$) for $\mathbf{v}_\infty = (3.90, 22.42, -1.55)$ km/s, ($\diamond$) for $\mathbf{v}_\infty = (6.90, 23.98, -2.35)$ km/s, and ($\square$) for $\mathbf{v}_\infty = (9.90, 25.21, -3.15)$ km/s. Around these bulk velocity vectors, denoted by ($+$), the circles with radii equal to one thermal speed are drawn

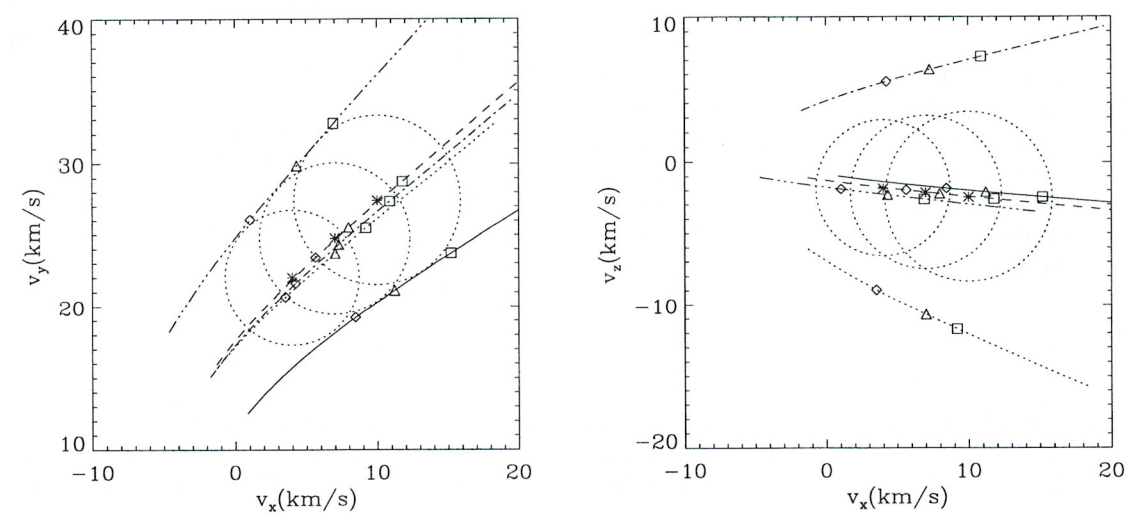

Fig. 10. Data set 2871.1B. The same plots as in Fig. 9. The viewing directions of the instrument are now: ($\epsilon = 54°, \alpha = 264°$) – solid line, ($\epsilon = 62°, \alpha = 248°$) – dotted line, ($\epsilon = 62°, \alpha = 264°$) – dashed line, ($\epsilon = 62°, \alpha = 280°$) – dashed-dotted line, and ($\epsilon = 70°, \alpha = 264°$) – dashed-triple_dotted line. The bulk velocity vectors and the corresponding $P_{\rm m}$ points are: $\mathbf{v}_\infty = (4.00, 22.02, -1.86)$ km/s for ($\triangle$), $\mathbf{v}_\infty = (7.00, 24.77, -2.16)$ km/s for ($\diamond$), and $\mathbf{v}_\infty = (10.00, 27.41, -2.47)$ km/s for ($\square$)

same relative distance (in units of $v_{\rm th}$) between the center of the distribution and the grid of $P_{{\rm m};ij}$ points. It happens to be possible in the case of 2871.1 data (Fig. 10), contrary to the case of 3601.2 (Fig. 9). One can say, that in the former case, the problem of determination the helium parameters is invariant with respect to a one-dimensional family of distribution function transformations in the velocity space. Any such transformation is a superposition of translation (change of $\mathbf{v}_{{\rm b};\infty}$), uniform deformation (change of T_∞), and scaling (change of n_∞). The different topology of $\mathbf{v}_{\infty;ij}(\tilde{v})$ lines for 3610.2 (curved sections) as compared with 2871.1 (straight sections) – see the (v_x, v_y) projections in Figs. 9 and 10, respectively – results from different gravitational deflection of particle orbits in the configuration space.

This leads us to the following interpretation. For the downwind spacecraft position at 1.5 AU in December 1990 the trajectories of helium atoms are strongly deflected from their asymptotic directions ($\mathbf{v}_\infty$). Moreover, in this case particles coming from different directions follow significantly different orbits (in terms of the orbital elements: perihelion distance, eccentricity, inclination). Hence, they originate from quite different parts of the distribution function at infinity. In such a case, the tomography problem can be solved within one observation. Contrary to this, in regions upstream of the Sun or at large distances (like in the second case – 2871.2) the gravitational effect is not sufficient to alter the orbital characteristics of the particles to that extend that the tomography problem can be solved with only one observation and a different method must be used.

5.3. *Solutions for ill-conditioned problems*

In order to determine the best solution in such an ill-conditioned problem we will investigate three different approaches. First, if we are sure that the unique set of helium parameters obtained from 3610.2 is correct, we can use it as a reference value $\mathbf{x}_{\rm ref}$ and find the point $\mathbf{x}_0$ closest to this value on the minimum line for 2871.1. We should, therefore, seek the minimum of:

$$d(\mathbf{x}_0, \mathbf{x}_{\rm ref}) = \sum_{i=1}^{4} \frac{(x_{0,i} - x_{{\rm ref},i})^2}{\sigma_i^2} \qquad (16)$$

The variances σ_i^2 can be taken from the a posteriori covariance matrix of parameters obtained for 3610.2 (see the paragraphs at the end of this section and Table 1). The density is excluded from the sum, since its apparent values can be different in both cases, due to potential changes in the efficiency function resulting from LiF evaporation between two measurements. The optimal parameters, obtained with this simple method for 2871.1, are presented in Table 1: lines 3 (NFOV) and 4 (WFOV).

Another approach for a unique determination of the neutral helium parameters consists of increasing the second term in the optimized function $S(\mathbf{x})$ (10). In this way we put some weak constraints on the parameters. We can change all or some of the variances $\mathbf{C}_{\mathbf{x}}^{-1}$. Again, the reference parameters are taken from the 3610.2 determination. For the reason explained above, the density and temperature should not be considered. The He parameters and the corresponding χ^2 obtained by increasing $\eta = \mathbf{C}_{\mathbf{x};ii}^{-1}$ monotonically from 1 to 10^5 for all three velocity components are presented in Fig. 11. χ^2 is defined as twice the first term in the optimized function (10). For the choice of η we use a criterion by Press et al. (1992), related to the χ^2 probability distribution. The expected value of the first term in (10) is equal to $\langle\chi^2\rangle = N-M$, while the variance is $\sigma_\chi^2 = 2(N-M) = 2\langle\chi^2\rangle$. Assuming a 1σ-error one should accept the solutions with $\chi^2 \leq \langle\chi^2\rangle + \sigma_\chi$. Unfortunately, χ_u^2 obtained by using unconstrained optimization for the 2871.1 data set is larger by 2σ than the expected value. Therefore, we modify the method slightly by accepting all η values that result in solutions with χ^2 not larger than $\chi^2 + 1\sigma$. To be specific, we use $\eta = 10^3$, in accordance with this criterion (Fig. 11). The results are presented in Table 1 (lines 5 and 6).

Finally, the third approach is to run the optimization program with both data sets simultaneously. This means we implicitly assume the same temperatures and velocities for both sets. The densities must be allowed to differ for the mentioned technical reasons, hence we increase the number of optimization parameters to 6. In this automatic method there are no arbitrary factors, the second term in (10) can be made very small. However, this method can be justified only if the underlying assumptions are correct, i.e. if the two data sets can be characterized by the same set of parameters at infinity. This does not represent a restriction on the physics of the interstellar neutral helium, which can be treated as stationary on the time scale of interest. The helium parameters obtained are shown in lines 7 and 8 of Table 1. They differ from the values obtained for any single data set. We suspect that this reflects the nonlinear nature of the optimization problem – the solution for the two data sets taken together is not a linear combination of the solutions for two data sets processed independently.

Following the idea of simultaneous processing of two or more data sets, we determine the values of parameters for the wide and narrow field-of-view measurements taken together (lines 7 to 11 in Table 1). The method is straightforward for 3610.2 but needs additional effort in the more difficult case of 2871.1. The idea of merging two subsets with different FOV is more easily justified than in the case of two different data sets - one should not expect any differences of physical parameters between the subsets. If the results are significantly different, it can only result from technical differences of two the detectors: slight mis-alignment of the optical axes, small differences in the efficiency function, etc.

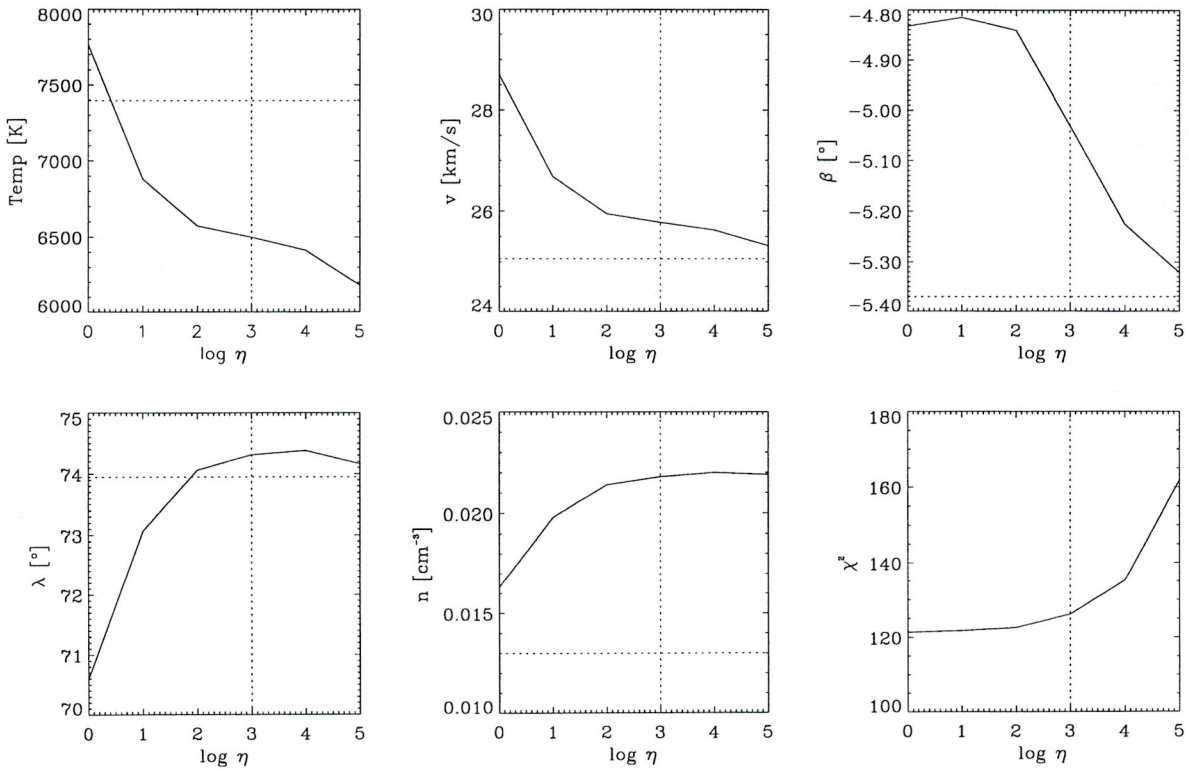

Fig. 11. Dependence of the best fit helium parameters on the model covariance coefficient η in the semi-automatic method for the 2871.1B data set. The horizontal dotted line corresponds to the reference values, obtained for 3610.2B. The vertical line corresponds to the standard value of $\eta = 10^3$ used in the calculations

According to our experience, method 2 (semi-automatic) provides the most reliable results and is and will be used preferentially in the data analysis.

5.4. *Error estimation*

Table 1 also contains the formal error bars and confidence levels calculated in Sect. 3. The errors for 2871.1 appear unrealistically large - as a the consequence of the ill-conditioned optimization problem. There is another method of evaluating the error bars: one can fix all, but one, best fit parameters and vary the remaining one to find how the average residuum $\rho = \sqrt{\frac{\chi^2}{N-M}}$ changes. The results for both data sets are presented in Figs. 12 and 13. To decide on a statistically acceptable level of the residuum increase we have to invoke again the χ^2 probability distribution. Since $\langle\chi^2\rangle = (N-M)$ and $\sigma_{\chi^2} = \sqrt{2(N-M)}$, we can accept $\Delta\rho = \rho - 1 < \frac{\sigma_{\chi^2}}{\langle\chi^2\rangle} = \sqrt{\frac{2}{N-M}}$. Substituting the numbers of pixels relevant for the 3610.2 and 2871.1 subimages one obtains $\Delta\rho = 20\%$ and $\Delta\rho = 15\%$ in the first and the second cases, respectively. This estimate, when applied to the plots presented in Fig. 12, for the 3610.2B data set, gives the error bars of helium parameters of the same order as the formal errors derived from the covariance matrix (Table 1). In the case of 2871.1B (Fig. 13) however, we obtain an independent evaluation of errors, not influenced by the ill-determined nature of the problem (compare with the formal error bars in Table 1).

6. Influence of non-optimized parameters

So far, we have not touched the problem of how the assumed, but not optimized, parameters of the model affect the results. They belong to two groups, related to instrumental effects ((1) and (2)), or to physical effects ((3) and (4)):

(1) spacecraft attitude and possible instrumental shifts of the elevation and/or azimuth;
(2) efficiency function;
(3) ionization rate;
(4) background value.

In fact, the values of these parameters can be determined from other sources (e.g. calibration, housekeeping data, etc.). However, any mistake in their determination gives rise to systematic errors in the helium parameters. To study this effect we computed the dependence of the results (He parameters) on the independent change of any of the above factors.

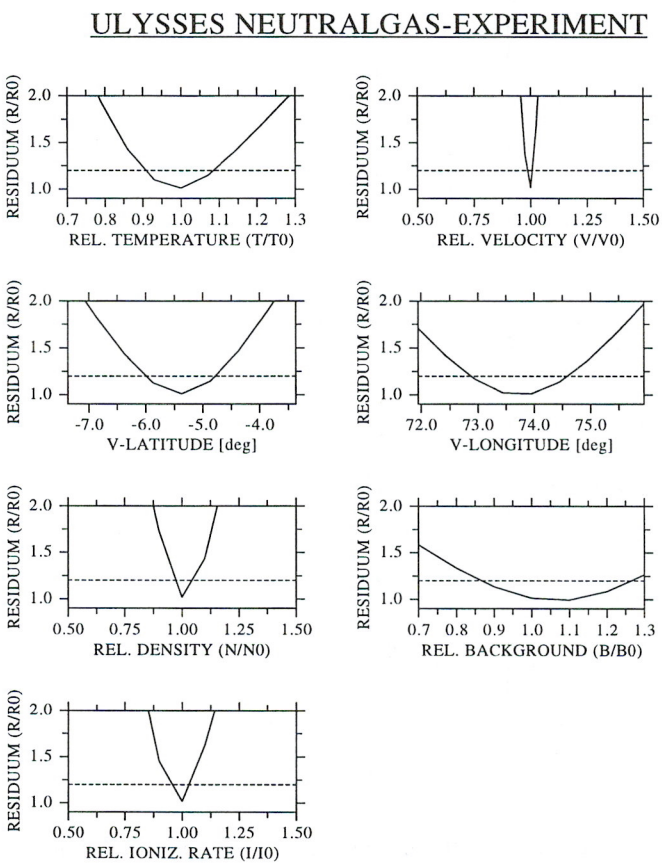

Fig. 12. Data set 3610.2B. Residuals as functions of the helium parameters at infinity. For each plot only one parameter is varied with respect to its reference value equal to the corresponding best fit parameter. The reference value of the residuum is given in $\langle\chi^2\rangle$ units, where $\langle\chi^2\rangle = N - M$ is the expected value of the residuum. This represents 1-dimensional cuts through the 5-dimensional residua-surface and demonstrates how well pronounced the absolute minimum is. The dashed line correspond to 1 σ_{χ^2} deviation from the expected value. The reference values are: $T_\infty = 7396$ K, $v_\infty = 25.06$ km/s, $\beta_\infty = -5\overset{\circ}{.}37$, $\lambda_\infty = 73\overset{\circ}{.}95$, $n_\infty = 0.013$ cm^{-3}, $\beta_{\rm ion} = 1.4\ 10^{-7}$ s^{-1}, and $Z_{\rm bckg} = 28.48$

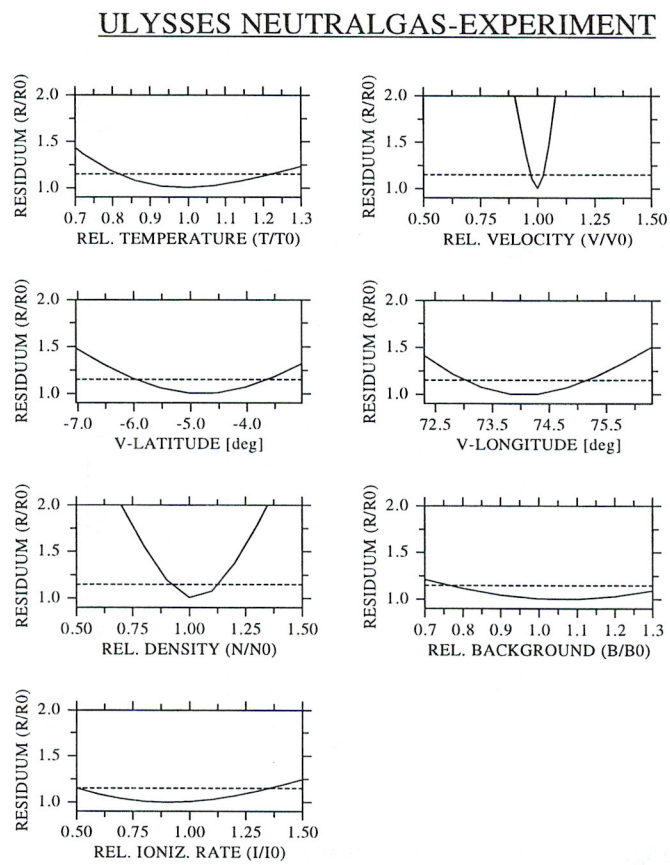

Fig. 13. Data set 2871.1B. The same plot as in Fig. 12. The reference values are: $T_\infty = 6499$ K, $v_\infty = 25.77$ km/s, $\beta_\infty = -5\overset{\circ}{.}03$, $\lambda_\infty = 74\overset{\circ}{.}31$, $n_\infty = 0.022$ cm^{-3}, $\beta_{\rm ion} = 1.4\ 10^{-7}$ s^{-1}, and $Z_{\rm bckg} = 33.99$. In this case the minima are much less pronounced than in the well determined case (Fig. 12)

6.1. *Azimuth and elevation shifts*

The attitude of Ulysses is determined and provided in navigation data files with an accuracy better than $0\overset{\circ}{.}5$. Any discrepancy between the assumed and real orientation of the spacecraft coordinate system can be described in terms of three angles, two of them corresponding to a difference in the spin axis direction (Fig. 14), and the third one being the angle between old and new x-axes. Considering only the effect of a spin axis change ($\Delta\beta$ or $\Delta\lambda$) we found for 3610.2 data set that the temperature and density are less affected than the other parameters, as one could expect: there is virtually no effect when $\Delta\beta$ is changed, while for $\Delta\lambda = 0\overset{\circ}{.}5$ the temperature and density vary by 250 K and 0.0013, respectively. On the other hand, the variations of β_∞ and λ_∞ are large: $2\overset{\circ}{.}1$ and $0\overset{\circ}{.}8$ for $\Delta\beta = 0\overset{\circ}{.}5$, or $5\overset{\circ}{.}0$ and $1\overset{\circ}{.}9$ for the same change of $\Delta\lambda$. The change of speed v_∞ is moderate and amounts to 0.2 km/s.

Another source of shifts in apparent values of helium parameters at infinity, which can be present even for a perfect attitude determination, consists in calibration inaccuracy of the reference (zero) positions of ϵ and α, and can be expressed as constant offsets of both angles: $\Delta\epsilon$, $\Delta\alpha$ with respect to the assumed values. In the case of 3610.2 we found that for the elevation shift $\Delta\epsilon = 1°$, the speed v_∞ can change by 1.8 km/s, λ_∞ by $1\overset{\circ}{.}1$, β_∞ by $0\overset{\circ}{.}4$, and the temperature T_∞ by 400 K. The shift in azimuth, $\Delta\alpha = 1°$, affects only β_∞ and λ_∞, by $1\overset{\circ}{.}4$ and $0\overset{\circ}{.}6$, respectively.

6.2. *Efficiency function*

Changes of the efficiency function are correlated only with the helium density. The product of efficiency and density is constant - in agreement with our expectations. The other

parameters are only slightly influenced; for example, 30% change in the efficiency function for 3610.2B results in < 10 K change of T_∞, < 0.04 km/s change of v_∞, $< 0.^\circ 2$ and $< 0.^\circ 1$ changes of β_∞ and λ_∞, respectively. It should be mentioned, however, that in our simulations we have simply re-scaled the efficiency functions by a constant factor; variations of the $f_{\rm eff}$ shape may have a larger effect on parameters other than the helium density.

6.3. *Ionization rate*

The maximum range for the ionization rate extends, most likely, from $\beta_{\rm ion} = 0.6\ 10^{-7}\ {\rm s}^{-1}$ (solar minimum) to $\beta_{\rm ion} = 1.6\ 10^{-7}\ {\rm s}^{-1}$ (solar maximum). The bulk velocity $\mathbf{v}_\infty$ and the temperature T_∞ depend only very weakly on $\beta_{\rm ion}$, the density n_∞ is, on the other hand, strongly correlated with the ionization rate, but this dependence gets less important for large heliocentric distances, because of the $1/r^2$ decrease of the solar UV-radiation field. Varying $\beta_{\rm ion}$ in the given range, we found that, at 1.55 AU downwind, n_∞ would vary from 0.0098 to 0.0205 cm^{-3} (3610.2A), from 0.0070 to 0.0165 cm^{-3} (3619.2B), and at 4.45 AU crosswind from 0.0166 to 0.0221 cm^{-3} (2871.1A), and from 0.0186 to 0.0239 cm^{-3} (2871.1B). In the case of the 2871.1 data sets we used the semi-automatic method of parameter determination with $\eta = 10^3$.

6.4. *Background*

As discussed in Sect. 4.5, the background is difficult to determine. Formally, the variance of the estimator (15) is $\sigma_Z^2 = Z^{\rm bckg}/\sqrt{K}$; in our cases when K is of the order of a few hundreds, σ_Z^2 is small. On the other hand, we have used a biased and insufficient estimator (Meyer 1975), and, therefore, we can expect that errors are markedly larger than σ_Z^2. It is likely, that the background values are underestimated for both data sets. We consider [27, 31] as a possible range of $Z^{\rm bckg}$ for 3610.2B. The corresponding ranges for 3610.2A, 2871.1B, and 2871.1A are: [14, 18], [32, 36], and [17, 21], respectively. An increase of $Z^{\rm bckg}$ from the lower to the upper limits of these intervals translates to a decrease in T_∞ by 800–1000 K for the NFOV data sets and a 300–400 K decrease for the WFOV. For the other parameters the variations are small: v_∞ can vary by 0.1–0.3 km/s (only for the 3610.2 data set), and n_∞ decreases by not more than 5% (WFOV) and 15% (NFOV).

7. Summary and conclusion

With the "interstellar neutral gas experiment" (GAS) on the ULYSSES spacecraft angular distributions of the interstellar neutral helium atoms have been measured in-situ and directly for the first time (Witte et al. 1992, 1993). First steps to determine the flow parameters of the He from these measurements have been described by Banaszkiewicz et al. (1990). Here we have three goals. First, to present the full description of the method of GAS data evaluation. Second, to show, for two different data sets, peculiarities of the specific inverse problem to solve and to give estimates of the accuracy of obtained results. Finally, we intended to show how the optimized parameters depend on input model parameters, which are known only approximately.

We have shown that the inverse method by Tarantola and the associated optimization method are valuable tools in the GAS data analysis. The numerical method of simulating the measured count numbers has been refined to give errors not larger than 2–3%, i.e. smaller than the statistical errors of measurements. The least accurate is determination of the background signal.

The related optimization problem is well-determined, i.e. has a unique solution, only for data sets obtained at Ulysses positions closer than 1.5 AU to the Sun and on the downwind side. At these points, the trajectories of incoming helium atoms have been gravitationally deflected strongly and in a different way for each direction of observation (pixel), therefore the whole observed image can be reproduced by the model for only one set of parameters of the Maxwellian distribution function at infinity. On the other hand, at distances larger than 3 AU in the crosswind direction, where the trajectories are not significantly differentiated by the gravitational force, the data sets cannot be uniquely inverted; one can obtain, at best, a line of solutions in the parameter space with almost the same (within the statistical error) value of the optimized function.

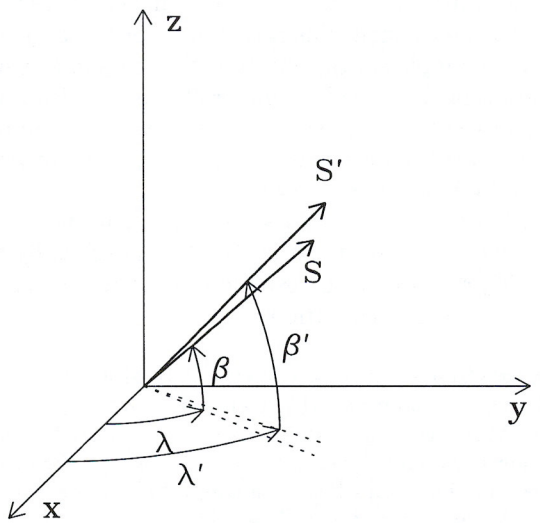

Fig. 14. The nominal (S) and actual (S') positions of the spin axis in the ecliptic (xyz) coordinate system. The errors in the attitude determinations are: $\Delta\beta = \beta' - \beta$ and $\Delta\lambda = \lambda' - \lambda$ (see text)

To solve this ill-conditioned problem we considered three different approaches. In the first one, a point on the

line is chosen as a solution when it is closest, in a certain range, to the reference values of the optimized function. The second, so called semi-automatic method employs a regularization term in the optimized function. This term increases quadratically with distance from the reference values. In the third, automatic, method two or more data sets, one of them with a unique solution, are processed together to determine a common best-fit set of He parameters. In our opinion, the second method is most reliable, even though one must use some a priori information about the possible solution. We have computed goodness-of-fit probabilities, which correspond to a high confidence level, so that the obtained results can be accepted. The error bars have been formally determined from the covariance matrix, i.e., they are meaningful only for well-determined problems.

After verifying that the estimated errors are within the expected limits for random fluctuations, we studied the possible systematic errors caused by uncertainities of model parameters, which are not subject to optimization. The ionization rate and efficiency function are anticorrelated with the helium density, but have only a small effect on velocity and temperature of helium atoms. An increase of the adopted background results in a decrease of the temperature, and in an increase in velocity and density. Finally, the attitude uncertainty affects mostly the speed and longitude values, at least for in-ecliptic measurements.

The calculations of the density, presented here, are based on the assumption that the loss rates (mainly due to photoionization) and the detection efficiency are constant. As it was mentioned, this is actually not quite the case for the two examples in this study and results in a systematic deviation in the density numbers (Table 1). However, the study of the longterm stability of these parameters is not subject to this paper as it does not affect the principles of the methods presented here.

In Witte et al. (1996) we will present the results for all in-ecliptic data sets either treated individually or combined in groups that correspond to the same observational and instrumental conditions.

Acknowledgements. We wish to thank E. Möbius, who acted as a referee, for many valuable comments and suggestions. One of us (M.B.) is very grateful to the Max-Planck Society for granting a stipend to participate in the ULYSSES/GAS data processing. This work has been supported by the Polish Committee for Scientific Research within the project no 2 Z6Z6001 05p13 and by the Deutsche Agentur für Raumfahrtangelegenheiten (DARA), GmbH, grant 50 ON 9103.

References

Axford W.I., 1972, in: Solar Wind II, NASA-Special Report SP-308, 609

Banaszkiewicz M., Rosenbauer H., Witte M., 1990, in: Physics of the Outer Heliosphere, COSPAR Coll. Ser. Vol. 1. In: Grzędzielski S., Page D.E. (eds.). Pergamon Press, p. 359

Chassefière E., Vial J.C., Lallement R., Bertaux J.L., Sandel B.R., 1990, in: Physics of the Outer Heliosphere, COSPAR Coll. Ser. Vol. 1. In: Grzędzielski S., Page D.E. (eds.). Pergamon Press, p. 65

Craig I.J.D, Brown J.C., 1986, Inverse Problems in Astronomy, Adam Hilger, Bristol

Fahr H.J., 1971, A&A 14, 263

Fahr H.J., 1990, in: Physics of the Outer Heliosphere, COSPAR Coll. Ser. Vol. 1. In: Grzędzielski S., Page D.E. (eds.). Pergamon Press, p. 327

Frisch P., 1990, in: Physics of the Outer Heliosphere, COSPAR Coll. Ser. Vol. 1. In: Grzędzielski S., Page D.E. (eds.). Pergamon Press, p. 19

Lallement R., 1990, in: Physics of the Outer Heliosphere, COSPAR Coll. Ser. Vol. 1. In: Grzędzielski S., Page D.E. (eds.). Pergamon Press, p. 49

Meier R.R., 1977, A&A 55, 211

Meyer S.L., 1975, Data Analysis for Scientists and Engineers. John Wiley & Sons Inc, New York

Möbius E., 1990, in: Physics of the Outer Heliosphere, COSPAR Coll. Ser. Vol. 1. In: Grzędzielski S., Page D.E. (eds.). Pergamon Press, p. 345

NAG Fortran Library, Mark 15, 1993, NAG Limited, Oxford

Parker R.L., 1977, Ann. Rev. Earth Planet. Sci. 5, 35

Press W.H., Teukolsky S.A., Vetterling W.T, Flannery B.P, 1992, Numerical Recipes, 2nd. ed., Cambridge University Press

Rosenbauer H., Fahr H.J., 1977, Direct measurements of the fluid parameters of the nearby interstellar gas using helium as tracer. Experiment Proposal for the Out-of-Ecliptic Mission, Internal Report, Max-Planck-Institut für Aeronomie, Katlenburg-Lindau, Germany

Tarantola A., 1987, Inverse Problem Theory. Elsevier, Amsterdam

Witte M., Rosenbauer H., Keppler E., Fahr H., Hemmerich P., Lauche H., Loidl A., Zwick. R., 1992, A&AS 92, 333

Witte M., Rosenbauer H., Banaszkiewicz M., Fahr H., 1993, Adv. Space Res. 93, 121

Witte M., Banaszkiewicz M., Rosenbauer H., 1996, in: The Heliosphere in the Local Interstellar Medium, von Steiger R., Lallement R., Lee M.A. (eds.), Space Sci. Rev. 78, 289

Wu F.M, Judge D., 1979, ApJ 231, 594